JMEPEG (2017) 26:4933–4939
DOI: 10.1007/s11665-017-2914-1

1059-9495/$19.00

Preparation and Mechanical Properties of TiC-Fe Cermets and TiC-Fe/Fe Bilayer Composites

Yong Zheng, Yang Zhou, Runfeng Li, Jiaqi Wang, Lulu Chen, and Shibo Li

(Submitted January 28, 2017; in revised form August 15, 2017; published online September 12, 2017)

TiC-Fe cermets and TiC-Fe/Fe bilayer composites consisting of a pure Fe layer and a TiC-Fe cermets layer were fabricated by hot-pressing sintering. The pure Fe layer contributes to the toughness of composites, and the TiC-Fe cermets layer endows the composites with an improved tensile strength and hardness. The effect of TiC contents (30–60 vol.%) on the mechanical properties of TiC-Fe cermets and TiC-Fe/Fe bilayer composites was investigated. Among the TiC-Fe cermets, the 40 vol.% TiC-Fe cermets possessed the highest tensile strength of 581 MPa and Vickers hardness of 5.1 GPa. The maximum fracture toughness of 17.0 MPa $m^{1/2}$ was achieved for the TiC-Fe cermets with 30 vol.% TiC. For the TiC-Fe/Fe bilayer composites, the 40 vol.% TiC-Fe/Fe bilayer composite owns the maximum tensile strength of 588 MPa, which is higher than that of 40 vol.% TiC-Fe cermets. In addition, the 33.5% increment of tensile strength of 30 vol.% TiC-Fe/Fe bilayer composite comparing with the 30 vol.% TiC-Fe cermets, which is attributed to the 30 vol.% TiC-Fe/Fe bilayer composite exhibited the largest interlaminar shear strength of 335 MPa. The bilayer composites are expected to be used as wear resistance components in some heavy wear conditions.

Keywords bilayer composites, hot-pressing, mechanical properties, microstructure, shear strength, TiC-Fe cermets

1. Introduction

Iron- and steel-based cermets reinforced with TiC particles exhibit combination of excellent physical and mechanical properties, such as low density, high hardness, improved strength and stiffness, and favorable wear property (Ref 1-5). Generally, the hardness and the wear resistance of cermets can be improved dramatically with increasing hard particles, whereas the toughness is rapidly decreased. The contradiction in mechanical properties makes this kind of cermet difficult to be processed into complicate components (Ref 6, 7). To solve this problem, the cermets are generally cladded to metals in order to make full use of the high hardness and wear resistance of cermets and high toughness of metals.

Research of cladding TiC-based cermets on steels and other alloys has been extensively performed. Many cladding methods, such as plasma spraying (Ref 8, 9), laser cladding (Ref 10), gas tungsten arc cladding (Ref 11) and chemical vapor deposition (Ref 12), could significantly improve wear resistance of substrates. However, these cladding layers exist pores and microcracks due to the thermal stress caused by temperature gradient with pure Fe or steel substrates. To meet the engineering requirements, many methods have been developed for cladding bulk cermets with metals, such as mechanical bonding (Ref 13), solid-state and liquid-state diffusion bonding (Ref 14, 15), reactive metal brazing (Ref 16), high energy beam welding and accumulative roll bonding (Ref 17). For example, Hu et al. (Ref 18) adopted field-activated pressure-assisted synthesis (FAPAS) method to bond TiC-TiB_2/Ni functional gradient materials (FGM) with Ti substrate using TiAl as the transitional layer. Huang et al. (Ref 19) applied combustion synthesis method in high-gravity field to combine TiC-TiB_2 ceramic with Ti-6Al-4 V alloy. Besides, Guo et al. (Ref 20) used plasma-activated sintering (PAS) to prepare 40Cr steels bonded with WC–Co cemented carbides using pure Ni as interlayers. To evaluate their mechanical properties, interlaminar shear strength is used to characterize the bonding strength. It was found that the interlaminar shear strength of the diffusion-bonded joint could be promoted as the original cladding surfaces were smooth (Ref 21). This is because the smooth surfaces are favorable for eliminating the interfacial interstices and microvoids.

Hot-pressing sintering is one of the most effective methods to bond bulk cermets with metal substrates. Through this method, it is possible to control the microstructure of bonded surface in the cermets for evaluating the interfacial bonding strength. Furthermore, the size of hard particles in cermet and the wettability with metal matrix are responsible for the interlaminar shear strength. It was reported that high-energy milling could effectively decrease particle size into submicron and even nanoscale. In addition, this process could also improve homogeneity of composition and promote sintering activity (Ref 22-24). It was also found that adding carbonyl iron powders into starting steel powders could promote the sintering activity (Ref 25).

In the literature, bilayer composites (BCs) and FGMs have been successfully prepared by hot-pressing sintering. Erdemir et al. (Ref 13) produced (30–60 wt.%) SiC/Al2024 BCs and FGMs by hot-pressing and consolidation method. Their studies showed that there were no indications of cracks within individual layers and of decohesion at interfaces. However, SiC-Al composites cannot be utilized in working conditions at above 600 °C due to the low melting point of Al. TiC-Fe cermets can cover the shortage of SiC-Al composites and be

Yong Zheng, Yang Zhou, Runfeng Li, Jiaqi Wang, Lulu Chen, and **Shibo Li**, Center of Materials Science and Engineering, School of Mechanical and Electronic Control Engineering, Beijing Jiaotong University, No. 3 Shangyuan Village, Haidian District, Beijing 100044, China. Contact e-mail: yzhou@bjtu.edu.cn.

used at above 1000 °C. However, the effect of TiC volume fraction on mechanical properties of TiC-Fe cermets and TiC-Fe/Fe BCs, especially on the interlaminar bonding strength and tensile strength of TiC-Fe/Fe BCs prepared by hot-pressing sintering, has not been investigated. Herein, we prepared TiC-Fe cermets and TiC-Fe/Fe BCs by hot-pressing sintering. The effect of TiC volume fraction on relative density, Vickers hardness, fracture toughness and tensile strength of TiC-Fe cermets was investigated. The microstructure, interlaminar shear strength and tensile strength of TiC-Fe/Fe BCs were also studied.

2. Experimental Procedures

2.1 Sample Preparation

TiC particles, reduced iron particles (RIP) and carbonyl iron particles (CIP) were used in the present work. The average particle size, purity and source of used raw materials are listed in Table 1. Fe matrix particles (consisted of 60 vol.% CIP and 40 vol.% RIP) and TiC particles (30, 40, 50 and 60 vol.%) were blended in a planetary ball miller (QM-3SP4) at room temperature in vacuum for 5 h using stainless steel jars with stainless steel balls. The milling speed was 300 rpm, and the ball-to-powder weight ratio was selected to be 10:1.

Hot-pressing sintering was used for preparing the pure RIP sample, TiC-Fe cermets and corresponding TiC-Fe/Fe bilayer composites (BCs), and all the samples were hot-pressed at 1270 °C under 25 MPa in argon atmosphere for 1 h. The sintered pure RIP sample was denoted as TC0, and the sintered TiC-Fe cermet samples with original TiC content of 30, 40, 50, 60 vol.% were denoted as TC30, TC40, TC50 and TC60, respectively. For the preparation of BCs, RIP particles were put in a graphite die coated with MgO, and an uniaxial pressure of 7 MPa was kept for 1 min to prepare a pure RIP layer, then TiC-Fe mixed particles were stacked on the RIP layer, and again the same pressure was brought to the die. The sintered TiC-Fe/Fe BCs samples were denoted as FTC30, FTC40, FTC50 and FTC60, respectively. The designation and composition of TiC-Fe cermets and TiC-Fe/Fe BCs are given in Table 2. No further thermal treatment was performed in the present study. Sintered samples were machined and polished with 2000 grit emery paper for the following tests.

2.2 Mechanical Property Test Procedure

The density of the sintered samples was measured by Archimedes method. Vickers hardness was measured (TH700) with a load of 2 kg for 15 s. The TiC-Fe cermets and TiC-Fe/Fe BCs (consisting an equal split of pure RIP layer and TiC-Fe cermet layer) were cut and ground into specimens as shown in Fig. 1(a) to test tensile strength. The TiC-Fe/Fe BCs were cut and polished into interlaminar shear strength specimens (Fig. 1b) with slotted holes in both sides to the interfacial region. The length of interfacial region between two layers is 1 mm. Fracture toughness of TiC-Fe cermets was tested by single-edge-notched beam specimens, as shown in Fig. 1(c). The tensile strength of TiC-Fe cermets and TiC-Fe/Fe BCs and the interlaminar shear strength of TiC/Fe BCs were measured in a universal testing machine (WDW-100) with a loading rate of 0.5 mm/min. The fracture toughness of TiC-Fe cermets was also tested in the universal testing machine with a loading rate of 0.05 mm/min.

Table 2 The designation and composition of TiC-Fe cermets and TiC-Fe/Fe BCs

Sample code	TiC, vol.%	CIP, vol.%	RIP, vol.%	Pure RIP layer
TC0	0	0	100	1
TC30	30	70 × 60%	70 × 40%	0
TC40	40	60 × 60%	60 × 40%	0
TC50	50	50 × 60%	50 × 40%	0
TC60	60	40 × 60%	40 × 40%	0
FTC30	30	70 × 60%	70 × 40%	1
FTC40	40	60 × 60%	60 × 40%	1
FTC50	50	50 × 60%	50 × 40%	1
FTC60	60	40 × 60%	40 × 40%	1

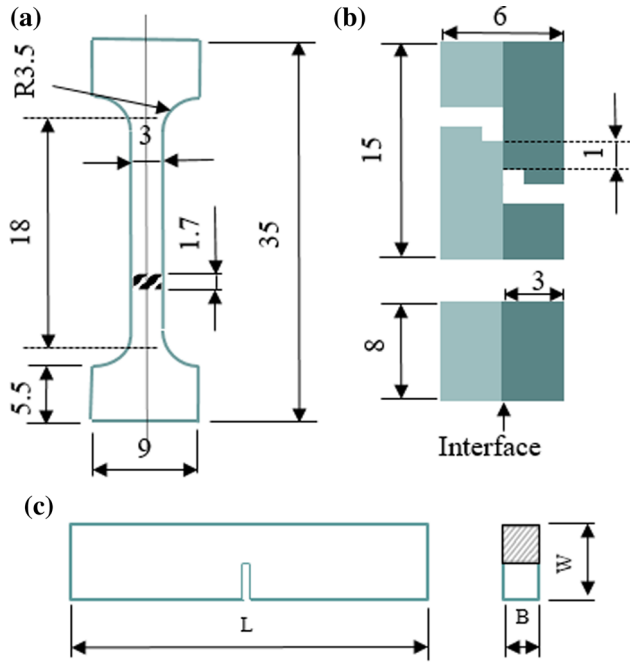

Fig. 1 Shape and size of the specimens used for (a) tensile test of TiC-Fe cermets and TiC-Fe/Fe BCs; (b) interlaminar shear test of bilayer composites; and (c) fracture toughness of TiC-Fe cermets (unit: mm)

Table 1 Average particle size, purity and source of used raw materials

Raw material	Average particle size, μm	Purity, %	Source
TiC	2–4	≥ 99	Zhuzhou Sanli Carbide Material Co., Ltd.
RIP	≤ 38	>99.2	Beijing Xing Rong Yuan Technology Co., Ltd.
CIP	3-5	>99.5	Beijing Xing Rong Yuan Technology Co., Ltd.

The fracture toughness K_{IC} (MPa·m$^{1/2}$) was calculated by the following formula:

$$K_{IC} = \frac{3PL}{2BW^2}\sqrt{a}\left(1.93 - 3.07\frac{a}{W} + 14.53\frac{a^2}{W^2} - 25.07\frac{a^3}{W^3} + 25.80\frac{a^4}{W^4}\right)$$

where P is the maximum load (N), L is the bearing distance (which is 20 mm in this case), B is the width of the specimens (mm), W is the thickness of the specimens, and a is the initial crack length. U-grooves for the fracture toughness tests were cut with the blade thickness of 0.25 mm from the sintered samples. Single-edge-notched beam specimens, with a precrack of a/W ratio of 0.4, were ground and polished to the final dimensions of 2.5 mm × 5 mm × 25 mm. At least three samples were used for each test to get average values of tensile strength, interlaminar shear strength and fracture toughness.

2.3 Phase Identification and Microstructures Observation

The phase identification of the milled blended particles and the sintered TiC-Fe cermets was characterized by x-ray diffraction (XRD) using Cu Ka radiation (D/Max-RB diffractometer). The microstructures were observed using a field emission scanning electron microscope (FESEM) equipped with an energy-dispersive spectrometer system (EDS). The interfacial structures between TiC and Fe in the sintered TiC-Fe cermets were investigated using a transmission electron microscope (TEM, FEI, F20).

3. Results and Discussion

3.1 TiC-Fe Cermets

Figure 2 presents XRD patterns of the milled blended particles and sintered sample of TC30; only TiC and α-Fe peaks are detected in these two cases. This suggests that there is no phase change during milling and sintering processes.

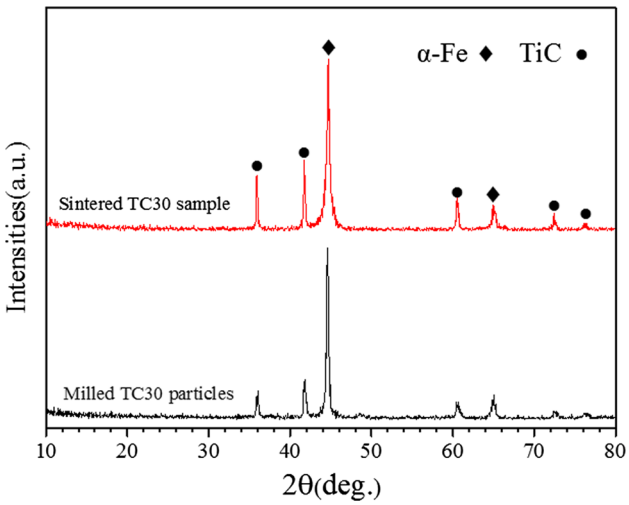

Fig. 2 XRD patterns of the milled blended particles and the sintered TC30 sample

Figure 3 shows the microstructure of the milled blended particles and the sintered sample of TC30. From Fig. 3(a), it can be seen that ball milling could effectively refine TiC particles which smashed into relatively huge RIP particles. Concerning about TC30 sample, Fig. 3(b) shows that the black phase (TiC) distributes uniformly in the gray phase (Fe) of the sample.

Figure 4 displays a representative TEM image of the TC40 and the high-resolution TEM (HRTEM) image of the dotted interface. Figure 4(a) confirms that no recation happened between α-Fe and TiC. Furthermore, no defects were found in the interfaces between these two phases. This suggests a fine bonding and endows composites with enhanced mechanical properties. The high-resolution TEM (HRTEM) image of the marked interface is shown in Fig. 4(b). The interplanar distances of TiC are 0.241 nm $(111)_{TiC}$ and 0.217 nm $(200)_{TiC}$, respectively. And the planar distance of Fe matrix is 0.203 nm $(110)_{Fe}$.

Figure 5 shows relative density and tensile strength of pure Fe layer (0 vol.% TiC) and TiC-Fe cermets (30–60 vol.% TiC). With the increase in TiC content, the relative density of TiC-Fe cermets is decreased. The TC30 possesses the highest relative density of 98.3%, while the TC60 has a lower relative density of 86.5%. As mentioned above, this is attributed to the fact that TiC particle clusters increased as the content of TiC increases, and higher sintering temperature and/or longer dwelling time is demanded to promote the rearrangement of hard particles and to attain high relative density. However, the relative density of

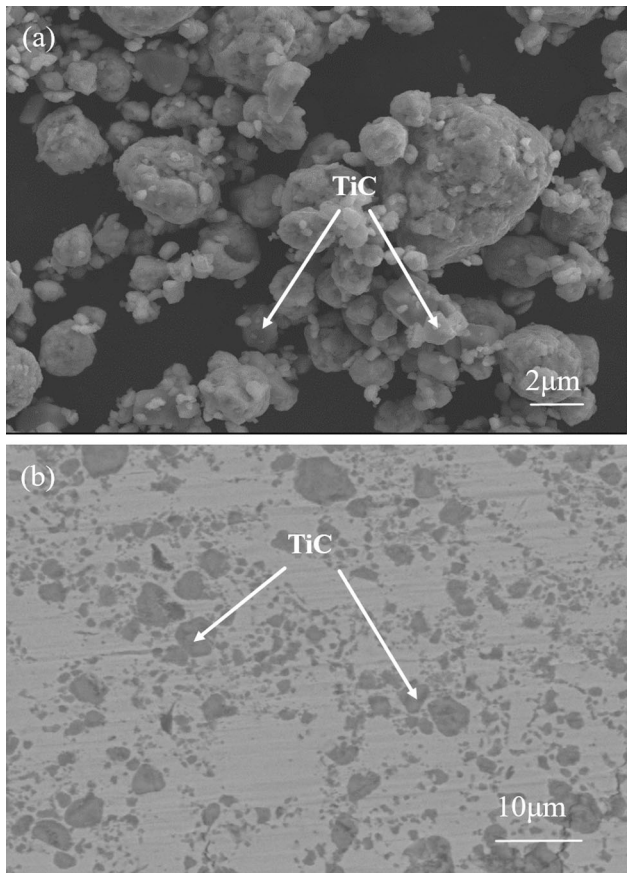

Fig. 3 SEM microstructures of (a) the milled blended particles and (b) the sintered sample of TC30

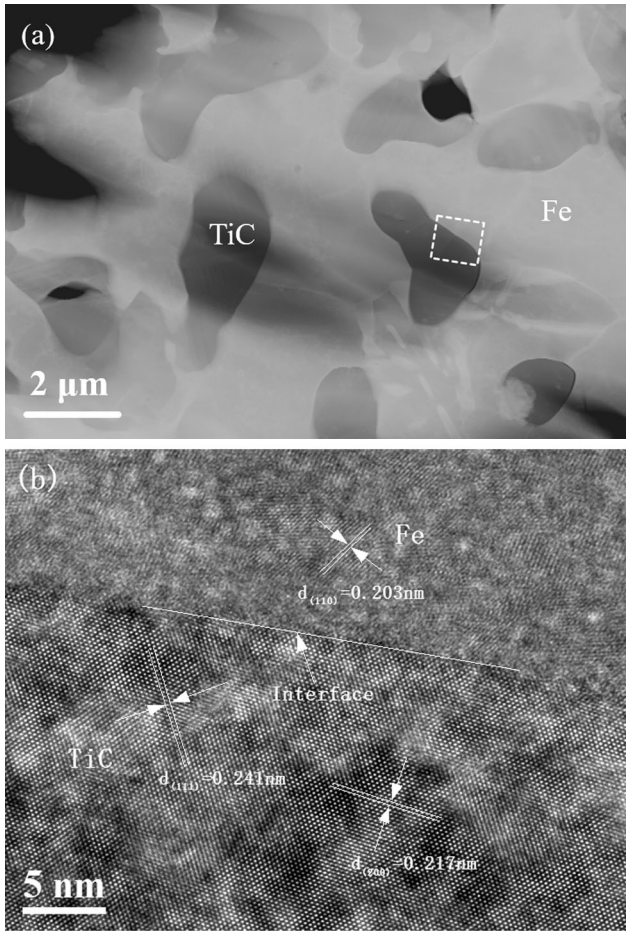

Fig. 4 (a) Typical TEM image of microstructure of TC40; (b) HRTEM image of the marked interface between TiC and Fe matrix

TC0 reaches 97.5%, which is lower than that of TC30 at the same sintering temperature. This is attributed to the promoting sintering effect of CIP (Ref 25). The tensile strength of TiC-Fe cermets increases with the increase in TiC content from 0 to 40%. The tensile strength of TC0 is approximately 296 MPa and that of TC40 peaks at 581 MPa. When TiC content is below 40%, the well-distributed TiC particles could effectively bear load transferred from Fe matrix and promote mechanical properties. However, the tensile strength decreased with further increase in TiC content, which should be induced by the TiC clusters. The tensile strength of TC50 and TC60 is 268 MPa and 121 MPa, respectively. These values are even lower than that of pure Fe.

Figure 6 shows the fracture toughness and Vickers hardness of TiC-Fe cermets. The maximum fracture toughness is 17.0 MPa $m^{1/2}$ when TiC content is 30 vol.%. The trend that fracture toughness decreases with the increase in TiC content remains. The average fracture toughness of TC40, TC50 and TC60 is 9.6, 6.6 and 3.2 MPa $m^{1/2}$, respectively. As can be seen from fracture surface of TC50 shown in Fig. 7, crack deflection, crack branch and crack bridge mechanism could effectively promote the fracture toughness of TiC-Fe cermets. TiC particles could induce the crack deflection and increase the length of crack propagation. It is well known that crack propagation is an energy absorption process, and thus the fracture toughness of brittle materials can be improved by the addition of second TiC phase (Ref 26). The hardness of

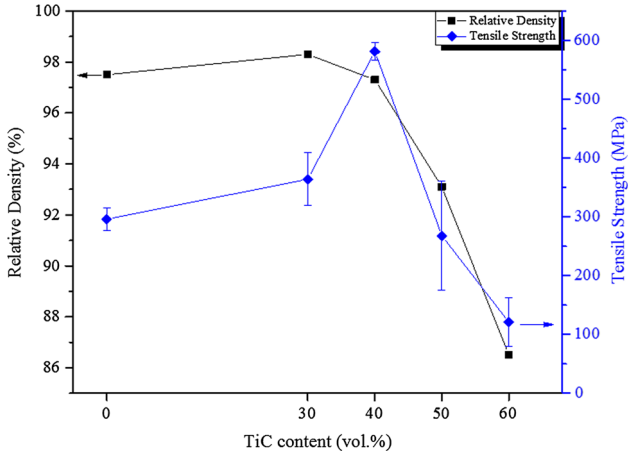

Fig. 5 Relative density and tensile strength of pure Fe layer and TiC-Fe cermets

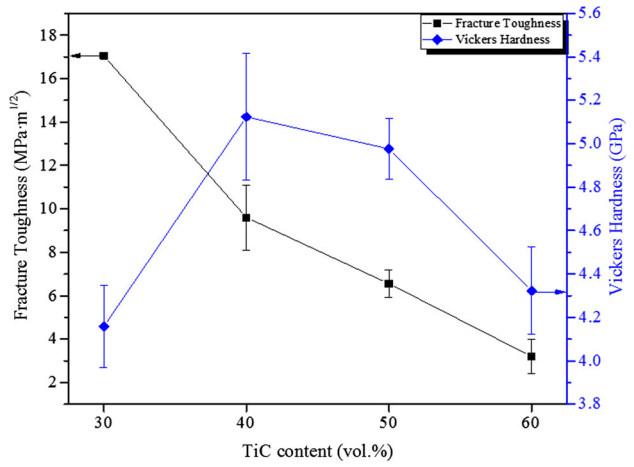

Fig. 6 Fracture toughness and Vickers hardness of TiC-Fe cermets

composites increased with the increase in TiC particles and reached to a peak value of 5.1GPa in TC40 sample. However, the hardness of TC50 and TC60 samples reduced instead of enhanced owning to lower relative density than TC40 sample, which was ascribed to the increment of TiCp agglomeration.

Typical fracture morphology of TC40 samples after tensile strength and fracture toughness test is shown in Fig. 8. Cubic morphology of TiC particles distributes uniformly in tensile TC40 sample (Fig. 8a). The fracture toughness morphologies of TC40 sample are shown in Fig. 8(b), displaying the presence of both intergranular fracture and transgranular fracture.

3.2 TiC-Fe/Fe Bilayer Composites

Figure 9 shows the interlaminar shear strength of bilayer composites composed of Fe layer and the different volume fraction of TiC-Fe cermets layer with the same thickness. The TiC volume fraction in the composite is directly taken from TiC-Fe cermets layer. It can be seen that an increase in TiC content in TiC-Fe cermets layer induces a reduction in the interlaminar shear strength of TiC-Fe/Fe BCs. The maximum interlaminar shear strength for FTC30 is up to 335 MPa. However, the shear strength of FTC60 is as low as 173 MPa. As the mismatch of the thermal expansion coefficient (CTE)

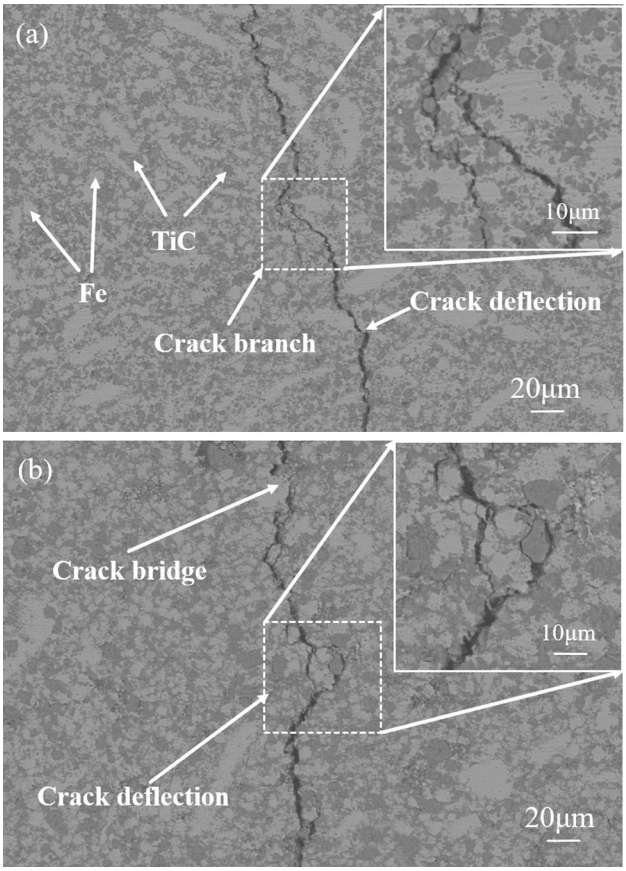

Fig. 7 SEM surface morphology of fracture toughness of TC50

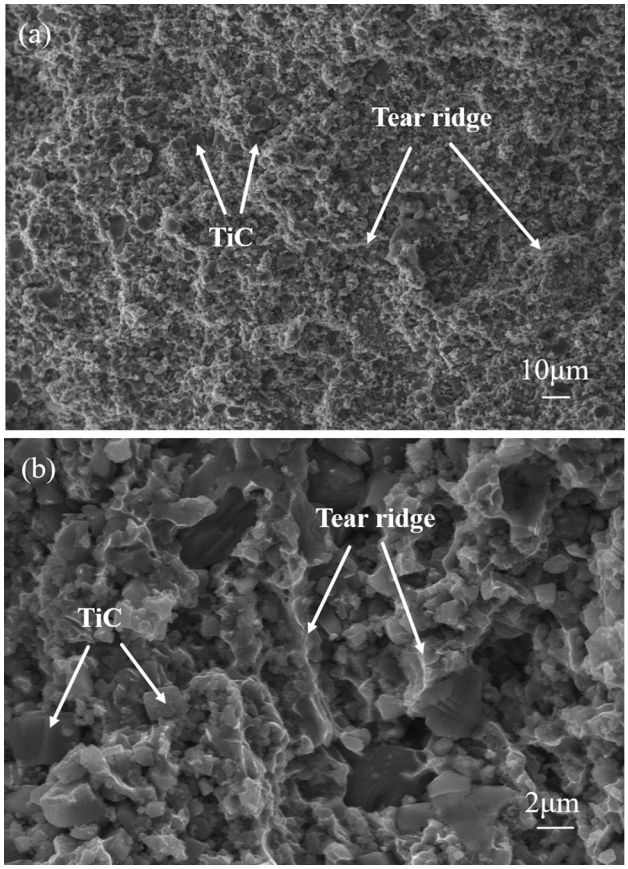

Fig. 8 Fracture morphology of TC40 samples after (a) tensile strength and (b) fracture toughness test

between TiC-Fe cermets layer and Fe layer can result in high residual thermal stresses, which originates during cooling process from the sintering temperature, the residual stresses increase when TiC content in composites layer increases. This has a huge effect on the interlaminar shear strength of bilayer composites. Accordingly, for successful bonding of cermet to metal, residual stress relief methods such as applying soft interlayer should be taken into consideration. Besides, it was found that the fracture occurred in the corresponding cermet layer after compression shear test, indicating that defects mainly distributed in the cermets layer.

The variation of Vickers hardness from pure Fe layer to TiC-Fe cermets layer in TiC-Fe/Fe BCs is shown in Fig. 10. Vickers hardness gradually increased with the increase in TiC content in TiC-Fe cermets for all bilayer composites. A sharply increment was found in the interfacial regions in the hardness curves, which indicates a well-bonded interface in the bilayer composites.

The cross-sectional surface images and fracture morphologies of FTC40 are shown in Fig. 11. Figure 11(a) indicates no phase transition happened between the pure Fe layer and TiC-Fe layer. No pores or microcracks were found at the interfacial region. Figure 11(b) shows that there are no pores or microcracks in both the fracture of the TiC-Fe cermets layer and the pure Fe layer. It also shows that TC40 layer exhibits brittle fracture mode, while pure Fe layer owns ductile fracture mode.

The tensile strength of TiC-Fe cermets and TiC-Fe/Fe bilayer composites is shown in Fig. 12. Comparing with the corresponding TiC-Fe cermets, the tensile strength of TiC-Fe/Fe bilayer composites owns the same variation trend and higher

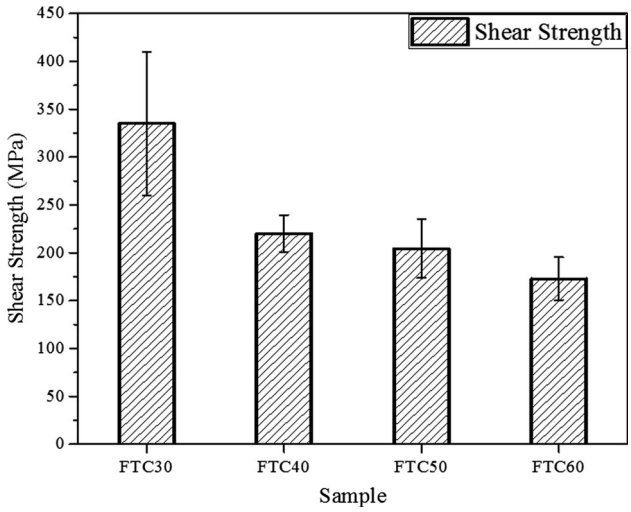

Fig. 9 Interlaminar shear strength of TiC-Fe/Fe bilayer composites

values except for FTC60. Overall, it means that the mechanical performance of TiC-Fe/Fe bilayer composites precedes or equals to the relevant TiC-Fe cermets layer, which could ensure to express the synergy effect between TiC-Fe cermets layer and pure Fe layer. It is very interesting that the tensile strength of FTC30 is 486 MPa, over 33.5% more than that of TC30, while the tensile strength of FTC40 and FTC50 increases slightly compared with the corresponding TC40 and TC50. It is

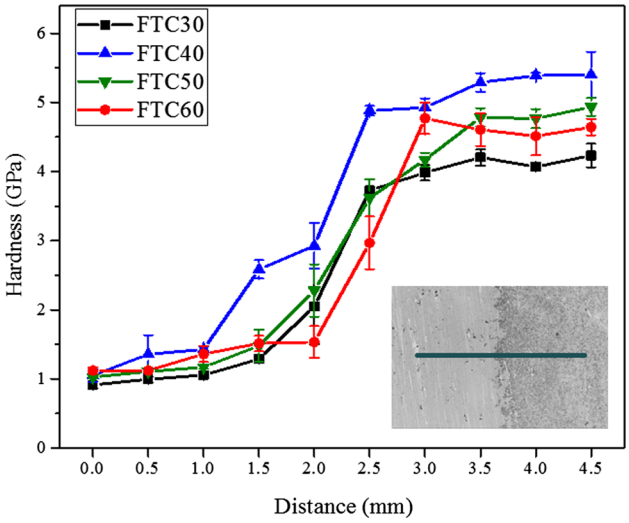

Fig. 10 Vickers hardness of TiC-Fe/Fe bilayer composites

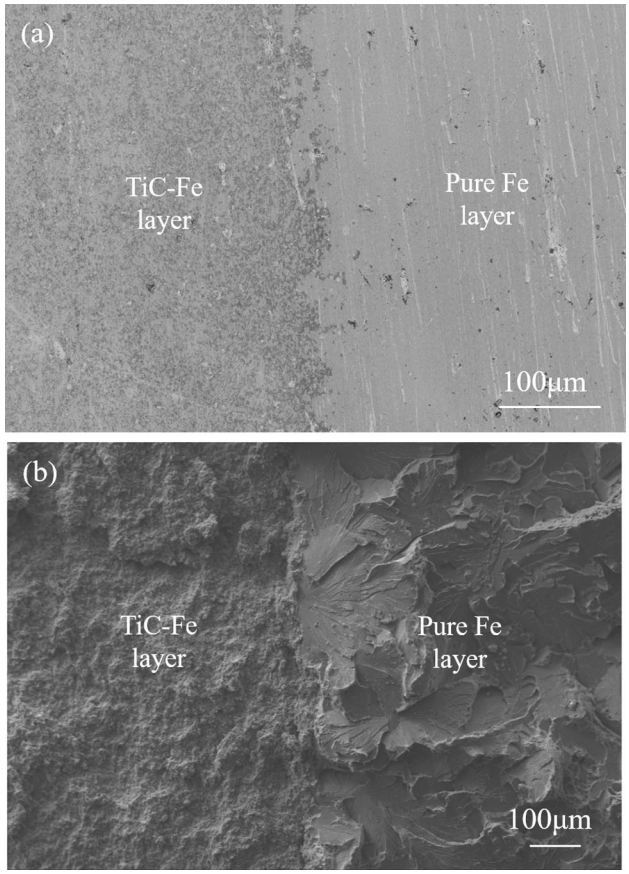

Fig. 11 (a) The cross-sectional surface images of the FTC40 bilayer composite; (b) the tensile fracture morphologies of the FTC40 bilayer composite

possible that the difference of elastic modulus between pure Fe layer and TiC-Fe cermets layer as well as their interlaminar shear strength caused the variation of tensile strength. When the same tensile load affects the bilayer composites, the pure Fe layer could generate longer deformation than TiC-Fe cermets layer. However, the strong interface bonding between two layers could cause compression stress in pure Fe layer and

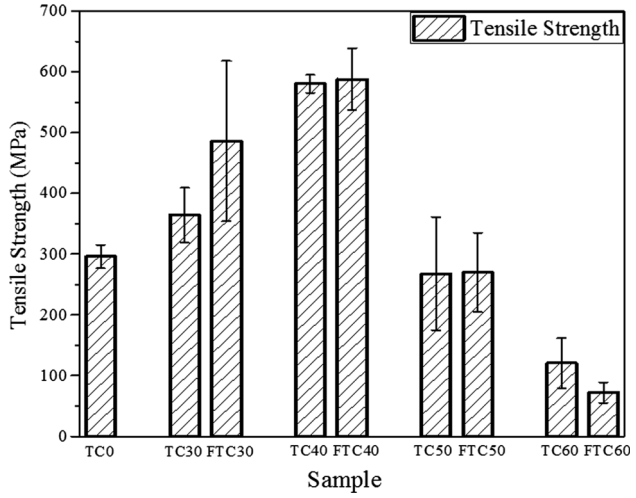

Fig. 12 Tensile strength of TiC-Fe cermets and TiC-Fe/Fe bilayer composites

tensile stress in TiC-Fe cermets layer, which has a synergy strengthen effect in the tensile strength of bilayer composites. The stronger the interface bonding, the more enhanced the tensile strength generated in each bilayer composite with corresponding TiC-Fe cermets layer. However, the tensile strength of FTC60 decreased because of weak interface bonding between pure Fe layer and TC60 layer.

4. Conclusions

TiC-Fe/Fe bilayer composites were fabricated by hot-pressing sintering at 1270 °C under 25 MPa in argon atmosphere for 1 h. There are no cracks and no decohesion at interfaces in the TiC-Fe/Fe bilayer composite, indicating the formation of strong bonding between pure Fe layer and TiC-Fe cermets layer. The relative density, Vickers hardness, tensile strength and fracture toughness of TiC-Fe cermets vary with different TiC volume fraction. The TiC-Fe cermets containing 40 vol.% TiC reach the highest tensile strength and Vickers hardness of 581 MPa and 5.1 GPa, respectively. The maximum fracture toughness is 17.0 MPa $m^{1/2}$ when TiC content is 30 vol.%. The interlaminar shear strength and tensile strength of TiC-Fe/Fe bilayer composites vary with TiC content in TiC-Fe cermets layer. TiC-Fe/Fe bilayer composites have a synergetic enhancement effect on mechanical properties than single TiC-Fe cermets. This is attributed to the strong interfacial bonding between TiC-Fe cermets layer and pure Fe layer. The maximum interlaminar shear strength is 335 MPa for 30 vol.% TiC-Fe/Fe bilayer composites. The maximum tensile strength is 588 MPa for 40 vol.% TiC-Fe/Fe bilayer composites. 30 vol.% TiC-Fe/Fe bilayer composites own the maximum increment of tensile strength of 33.5% compared with that of corresponding TiC-Fe cermets than other TiC-Fe/Fe bilayer composites.

Acknowledgments

This work was supported by the National Natural Science Foundation of China under Grant Nos. 51472024, 51172015, 51372015.

Conflict of interest

The authors declare that they have no conflict of interest.

References

1. K. Das, T.K. Bandyopadhyay, and S. Das, A Review on the Various Synthesis Routes of TiC Reinforced Ferrous Based Composites, *J. Mater. Sci.*, 2002, **37**, p 3881–3892
2. K.I. Parashivamurthy, R.K. Kumar, S. Seetharamu, and M.N. Chandrasekharaiah, Review on TiC Reinforced Steel Composites, *J. Mater. Sci.*, 2001, **36**, p 4519–4530
3. D.P. Yi, P.C. Yu, B. Hu, H.Q. Liu, B. Wang, and Y. Jiang, Preparation of Nickel-Coated Titanium Carbide Particulates and their Use in the Production of Reinforced Iron Matrix Composites, *J. Mater. Des.*, 2013, **52**, p 572–579
4. N.R. Oh, S.K. Lee, K.C. Hwang, and H.U. Hong, Characterization of Microstructure and Tensile Fracture Behavior in a Novel Infiltrated TiC–Steel Composite, *J. Scripta Mater.*, 2016, **112**, p 123–127
5. Z. Wang, T. Lin, X.B. He, H.P. Shao, B. Tang, and X.H. Qu, Fabrication and Properties of the TiC Reinforced High-Strength Steel Matrix Composite, *J. Refract. Met. Hard Mater.*, 2016, **58**, p 14–21
6. X.H. Zhang, J. Yang, J.Q. Ma, Q.L. Bi, J. Cheng, Y.M. Liang, and W.M. Liu, Microstructures and Mechanical Properties of Fe–28Al–5Cr/TiC Composites Produced by Hot-Pressing Sintering, *J. Mater. Sci. Eng. A*, 2011, **528**, p 6819–6824
7. E. Pagounis, M. Talvitie, and V.K. Lindroos, Influence of the Metal/Ceramic Interface on the Microstructure and Mechanical Properties of HIPed Iron-Based Composites, *J. Compos. Sci. Technol.*, 1996, **56**, p 1329–1337
8. L.C. Betancourt-Dougherty and R.W. Smith, Effects of Load and Sliding Speed on the Wear Behaviour of Plasma Sprayed TiC-NiCrBSi Coatings, *J. Wear*, 1998, **217**, p 147–154
9. H.T. Wang, J.H. Huang, J.L. Zhu, H. Zhang, and X.K. Zhao, Microstructure of Composites Coating Prepared by Plasma Spraying of Fe–Ti–C Powder Using Sucrose as Carbonaceous Precursor, *J. Alloys Compd.*, 2009, **472**, p 1–5
10. J.M. Wilson and Y.C. Shin, Microstructure and Wear Properties of Laser-Deposited Functionally Graded Inconel 690 Reinforced with TiC, *J. Surf. Coat. Technol.*, 2012, **207**, p 517–522
11. M. Sharifitabar, J. Vahdati KhakiM, and Haddad Sabzevar, Microstructure and Wear Resistance of In Situ TiC–Al_2O_3 Particles Reinforced Fe-Based Coatings Produced by Gas Tungsten Arc Cladding, *J. Surf. Coat. Technol.*, 2016, **285**, p 47–56
12. M. Azadi, A. Sabour Rouhaghdam, S. Ahangarani, and H.H. Mofidi, Mechanical Behavior of TiN/TiC Multilayer Coatings Fabricated by Plasma Assisted Chemical Vapor Deposition on AISI, H13 Hot Work Tool Steel, *J. Surf. Coat. Technol.*, 2014, **245**, p 156–166
13. F. Erdemir, A. Canakci, T. Varol, and S. Ozkaya, Corrosion and Wear Behavior of Functionally Graded Al2024/SiC Composites Produced by Hot Pressing and Consolidation, *J. Alloys Compd.*, 2015, **644**, p 589–596
14. J. Li, G.M. Sheng, and L. Huang, Ti–Nb–Cu Stress Buffer Layer for TiC Composites/304 Stainless Steel Diffusion Bonding, *J. Rare Met. Mater. Eng.*, 2016, **45**, p 555–560
15. Z.X. Guo, H. Zhong, M. Yang, J. Xiong, W.C. Wan, and M.X. Liang, Microstructure and Properties of the Ti(C, N)–xMo2C–Ni Composites/Steel Joint by a Novel Diffusion Bonding Method, *J. Mater. Charact.*, 2015, **99**, p 92–100
16. R. Johari Miab and A.M. Hadian, Effect of Brazing Time on Microstructure and Mechanical Properties of Cubic Boron Nitride/Steel Joints, *J. Ceram. Int.*, 2014, **40**, p 8519–8524
17. Majed Zabihi, Mohammad Reza Toroghinejad, and Ali Shafyei, Shear Punch Test in Al/Alumina Composite Strips Produced by Powder Metallurgy and Accumulative Roll Bonding, *J. Mater. Sci. Eng. A*, 2016, **667**, p 383–390
18. L.F. Hu, D.M. Chen, Q.S. Meng, and H. Zhang, Microstructure Characterization and Mechanical Properties of (TiC–TiB_2)–Ni/TiAl/Ti Functionally Gradient Materials Prepared by FAPAS, *J. Alloys Compd.*, 2015, **636**, p 298–303
19. X.G. Huang, Z.M. Zhao, and L. Zhang, Fusion Bonding of Solidified TiC-TiB_2 Ceramic to Ti–6Al–4 V Alloy Achieved by Combustion Synthesis in High-Gravity Field, *J. Mater. Sci. Eng. A*, 2013, **564**, p 400–407
20. Y.J. Guo, Y.Q. Wang, B.X. Gao, Z.Q. Shi, and Z.W. Yuan, Rapid Diffusion Bonding of WC-Co Cemented Carbide to 40Cr Steel with Ni Interlayer: Effect of Surface Roughness and Interlayer Thickness, *J. Ceram. Int.*, 2016, **42**, p 16729–16737
21. A. Laik, P. Mishra, K. Bhanumurthy, G.B. Kale, and B.P. Kashyap, Microstructural Evolution During Reactive Brazing of Alumina to Inconel 600 using Ag-Based Alloy, *J. Acta Mater.*, 2013, **61**, p 126–138
22. M. Sheikhzadedh and S. Sanjabi, Structural Characterization of Stainless Steel/TiC Nanocomposites Produced by High-Energy Ball-Milling Method at Different Milling Times, *J. Mater. Des.*, 2012, **39**, p 366–372
23. Y.B. Fu, Z.J. Wang, and A.J. Xu, Al_2O_3 Nanoparticles Induced High Dezincification Corrosion Resistance of 71 wt.% Cu–Zn alloy, *J. Sci. Adv. Mater.*, 2015, **7**, p 2570–2575
24. Y.B. Fu, Y.P. Lu, Z.J. Wang, Z.Q. Cao, and A.J. Xu, Microstructural Refinement and Performance Improvement of Cu-36 wt.% Zn Alloy by Al_2O_3 Nanoparticles Coupling Electromagnetic Stirring, *J. Rare Met.*, 2016, **8**, p 1–6
25. Y.J. Xiong, X.B. Li, R.T. Liu et al., Influences of Hot Isostatic Pressing Technology on Microstructure and Abrasion Properties of a New Steel Bonded Titanium Carbide, *J. Lubric Eng.*, 2007, **32**, p 85–87
26. Y.P. Bai, J.D. Xing, Y.C. Guo, J.P. Li, Y.Y. He, and S.Q. Ma, Effect of Cr on Microstructure, Mechanical Properties, and Wear Behavior of In Situ 20 wt.% Al_2O_3/Fe-25Al Composites, *J. Mater. Eng. Perform.*, 2015, **24**, p 936–945